Biophysical Journal
Article

Biophysical Society

Cholesterol Partition and Condensing Effect in Phase-Separated Ternary Mixture Lipid Multilayers

Yicong Ma,[1] Sajal K. Ghosh,[1] David A. DiLena,[1] Sambhunath Bera,[1] Laurence B. Lurio,[2] Atul N. Parikh,[3] and Sunil K. Sinha[1,*]

[1]Department of Physics, University of California-San Diego, La Jolla, California; [2]Department of Physics, Northern Illinois University, DeKalb, Illinois; and [3]Department of Biomedical Engineering and Department of Chemical Engineering and Materials Science, University of California-Davis, Davis, California

ABSTRACT The cholesterol partitioning and condensing effect in the liquid-ordered (L_o) and liquid-disordered (L_d) phases were systematically investigated for ternary mixture lipid multilayers consisting of 1:1 1,2-dipalmitoyl-*sn*-glycero-3-phosphocholine/1,2-dioleoyl-*sn*-glycero-3-phosphocholine with varying concentrations of cholesterol. X-ray lamellar diffraction was used to deduce the electron density profiles of each phase. The cholesterol concentration in each phase was quantified by fitting of the electron density profiles with a newly invented basic lipid profile scaling method that minimizes the number of fitting parameters. The obtained cholesterol concentration in each phase versus total cholesterol concentration in the sample increases linearly for both phases. The condensing effect of cholesterol in ternary lipid mixtures was evaluated in terms of phosphate-to-phosphate distances, which together with the estimated cholesterol concentration in each phase was converted into an average area per molecule. In addition, the cholesterol position was determined to a precision of ($\pm$0.7Å) and an increase of disorder in the lipid packing in the L_o phase was observed for total cholesterol concentration of 20~30%.

INTRODUCTION

The raft hypothesis of biological membranes, first advanced now more than two decades ago, continues to invoke considerable debate and controversy (1–4). Its central claim has been that the lipid bilayer in cellular membranes is not an unstructured solvent; rather it is chemically textured, consisting of phase-separated domains enriched in saturated lipids, cholesterol, sphingolipids, and certain integral membrane proteins (e.g., GPI-anchored proteins, SRC kinases). The hypothesis is based on the experimental observations that insoluble membrane fragments—resistant to disruption by Triton X-100 at 4°C—are generally enriched in saturated lipids and cholesterol. This led to the proposition that these detergent-resistant membrane fragments correspond to discrete raft domains within cell membranes. Because the physical state of the membrane is most likely altered in going from the physiological 37°C to the 4°C used for detergent solubilization, the notion that detergent-resistant membrane correspond to identifiable membrane domains in living cells has been largely discredited. However, extensive search over the past two decades for microdomains has brought the question of how cholesterol mixes with membrane lipids into a sharp, renewed focus.

In the absence of cholesterol, essentially cylindrically shaped phospholipids, saturated or unsaturated, adopt a bilayer motif. Below their main phase transition temperature (T_m), the bilayers (typically composed of saturated lipids) exist in a gel (or solid) state characterized by tight packing of conformationally ordered, extended acyl chains. When the bilayer T_m is lower than the membrane temperature, such as for many unsaturated lipids, conformationally disordered chains in loose packing characterize two-dimensionally fluid bilayers. The nonideal mixing of cholesterol, first reported in 1925 by Leathes (5), with saturated (or unsaturated) lipids, profoundly influences molecular packing generating new phases: when added to high-melting saturated lipids, cholesterol perturbs the tight packing of the gel phase exerting fluidizing effect and transforming the gel phase, above a threshold concentration, into a new liquid-ordered (L_o) phase. By contrast, cholesterol association with the fluid phase phospholipids above T_m produces a condensing effect, by intercalating between loosely

Submitted April 14, 2015, and accepted for publication February 16, 2016.

*Correspondence: ssinha@physics.ucsd.edu

Sajal K. Ghosh's present address is Department of Physics, Shiv Nadar University, Chithera, Dadri, Gautam Budh Nagar, India.

Sambhunath Bera's present address is Amity University-UP, Sector-125, Noida, India.

Editor: Tobias Baumgart.

http://dx.doi.org/10.1016/j.bpj.2016.02.022

packed acyl tails and ordering neighboring chains. In other words, cholesterol fluidizes the gel phase of saturated lipids and condenses fluid phases of unsaturated lipids, driving each toward an intermediate L_o phase characterized by intermediate packing density and membrane fluidity.

In multicomponent lipid mixtures, consisting of both saturated and unsaturated lipids, then, the phase behavior is determined by the balance of quantitative distribution of cholesterol between the two lipid types. In the work reported here, we report x-ray diffraction measurements in conjunction with a newly developed (to our knowledge) modeling procedure to extract detailed, quantitative information regarding cholesterol distribution in ternary mixtures containing a saturated and an unsaturated lipid in a hydration-controlled smectic lipid multilayer. We find that cholesterol associates in greater concentrations with the saturated phospholipid-stabilizing L_o phase within the L_d-surrounding three-dimensional phase.

Phase diagrams of ternary lipid mixtures consisting of saturated lipids, unsaturated lipids, and cholesterol have been studied systematically by Veatch and Keller (6–8) and Veatch et al. (9) mainly using fluorescence microscopy. NMR was used to determine tie lines in the phase diagrams (10). Moreover, Heftberger et al. (11) and Uppamoochikkal et al. (12) have reported phase diagrams and the effect of cholesterol in a similar system by using small angle x-ray scattering technique. There are also x-ray scattering studies in attempts to determine the composition of coexisting phases by Chen et al. (13).

A lot of studies on the cholesterol effect were carried out from different angles. Solubility of cholesterol in lipid membranes were reported by Barrett et al. (14), as well as cholesterol effects on drug molecules such as ibuprofen, by Alsop et al. (15).

In the cholesterol-induced phase separation processes, the role of condensing effect due to cholesterol remains unclear. Although the condensing effect of cholesterol in binary systems has been studied systematically (16–19), no systematic and quantitative studies have been carried out to measure the condensing effect in ternary systems, nor its relation to cholesterol-induced phase separation. To do that, we carried out x-ray diffraction studies on supported multilayer of lipid mixtures consisting of saturated lipid, unsaturated lipid, and cholesterol, and used quantitative modeling of the electron density profiles (EDP) to extract such information.

X-ray and neutron lamellar diffraction methods applied to lipid multilayers have been well established and demonstrated as powerful techniques to quantitatively study the detailed lipid bilayer structures, as explained in the review article by Pabst et al. (20). Using these methods, cholesterol packing structures with several different kinds of lipids have been studied (21,22). Diffraction data usually are converted to electron density profiles, and decomposed into different chemical group densities with modeling (23), sometimes with the help of molecular simulations (24,25). In this study of mixed lipid multilayer systems with cholesterol, we propose a simple yet effective modeling scheme that helps to quantify the composition and localize the cholesterol positional distribution with Ångstrom accuracy.

MATERIALS AND METHODS

DPPC (1,2-dipalmitoyl-*sn*-glycero-3-phosphocholine) and DOPC (1,2-dioleoyl-*sn*-glycero-3-phosphocholine) solutions were purchased from Avanti Polar Lipids (Alabaster, AL) with accurate concentrations of the lipids specified. Cholesterol was purchased from Sigma-Aldrich (St. Louis, MO). All the purchased chemicals were used without further purification. The phospholipids and cholesterol were mixed in the desired proportions and dissolved in a chloroform and TFE (tetrafluoroethylene) 1:1 mixture solvent (26), to yield a final concentration 8 mg/mL.

Silicon substrates, cut to 17 × 20 mm wafers, were first sonicated for 15 min in methanol followed by another 15 min in deionized water (18 M-Ohm cm^{-1}, Milli-Q; Millipore, Billerica, MA). Substrates were then nitrogen-dried, and exposed to short-wavelength UV radiation for ~15 min to make the surface hydrophilic. The prepared substrates were then placed on a carefully leveled platform for lipid deposition. One-hundred microliters of lipid solution were deposited on each substrate and covered by a large Petri dish for slow evaporation in the fume hood. After 3~4 h, the samples were transferred to a vacuum chamber for 36 h to remove remaining traces of solvent. After removing from the vacuum, the samples were placed in humidity chambers maintained at 96% relative humidity (RH) at 50°C and incubated for 48 h.

Subsequently, the samples are cooled to room temperature at the ambient rate. Depending on the lipid composition, samples equilibrate to a uniform multibilayer or phase separate into two coexisting lamellar phases (a DPPC-rich L_o phase and a DOPC-rich L_d phase). Consistent with our earlier findings, equilibration of phase-separating lipid mixtures involves thickness-dependent lateral coarsening of the domains and interlayer domain registration producing a columnar mesophase (27). Depending on the humidity in the chamber and sample thickness, the domain equilibration process given above takes one to several days to complete. The diffraction measurements were carried out after the registering process was mostly complete.

Although elaborate, the procedure above ensures reproducibility in producing a high quality of samples as reflected by the observations of up to the ninth order of diffraction peaks with an in-house x-ray tube source. A sample set consisting of a fixed 1:1 DPPC/DOPC containing systematically varied molar fraction cholesterol (0, 10, 16, 20, 25, and 30%) was prepared (e.g., for the 16% cholesterol sample, the composition is 42:42:16% DPPC/DOPC/cholesterol in molar ratio) and characterized. This cholesterol molar fraction will be denoted with $\mathbf{\Phi_c}$ in later uses. All samples were measured at room temperature (~25°C), except for the sample containing 30% cholesterol, which was measured at 11°C due to a much lower phase transition temperature of this specific mixture (~20°C), as shown by Mills et al. (28).

RESULTS

X-ray diffraction

X-ray diffraction measurements were carried out using an in-house Cu K_α tube spectrometer with wavelength 1.54 Å operating in the horizontal plane. Beam dimensions were set to be 0.2 mm in the horizontal direction and wide open (10 mm) in the vertical direction. Our custom-designed humidity chamber (29), which can control RH to 0.01% accuracy close to full hydration when used as a high humidity control chamber, was used for the measurements. The chamber was loaded with a saturated salt solution of K_2SO_4 to keep

the samples at a fixed partial hydration under 97% RH at a room temperature of 25°C during measurements (with an exception of 30% cholesterol at 11°C, as explained in the Materials and Methods).

Because of the high degree of registration for each of the two coexisting phases, the phase-separated sample yields several orders of diffraction peaks (up to nine orders for the L_o phase). Polarization corrections and absorption corrections were applied to the data collected. The lineshapes of multilayer diffraction peaks are often fitted by expressions due to Caille (30). However, we did not observe Caille line shapes here, probably due to the partial hydration condition, which result in suppressed interlayer fluctuations. Thus, the diffraction peaks were fitted to Gaussians after subtracting a sloping background. The integrated intensity I_n of nth order peaks were then used to calculate the electron density profiles with the following equation (31):

$$\rho_{\text{relative}}(z) = \frac{2}{d}\sum_n v(n) n \sqrt{I_n} \cos\left(\frac{2\pi n z}{d}\right), \qquad (1)$$

where d is the lamellar spacing, $v(n)$ is the phase factor for the nth order reflection, and the factor n arises from the Lorentz correction of q_z^{-2} applied to the raw intensities I_n, as suggested by Li et al. (26). Because of the mirror symmetry of the bilayers in the z direction, it can be shown that the phase factors can only be ± 1. For each phase, intensities of all diffraction orders are normalized by the sum of all peak intensities in that phase to account for the full beam intensity normalization correction. This correction is essential before the electron density profile is normalized to an absolute scale, using the method described in the next section.

Absolute electron density profile generation

To extract quantitative information of cholesterol content from the electron density profiles, correct phase choices for every diffraction order and proper normalization to an absolute scale are both required.

Phasing

Lipid samples with 0, 16, 20, and 25% cholesterol ($\mathbf{\Phi_c}$) were measured under three different hydrations (with saturated salt solution as reservoir): 84% (KCl), 94% (K_2NO_3), and 97% (K_2SO_4) RH so that the swelling method (32,33) could be used to determine the phases. A representative set of diffraction patterns of 0% cholesterol sample measured at room temperature under different hydrations is shown in Fig. 1 *a*. An example of phasing diagrams for the same sample is shown in Fig. 2. Additional phasing diagrams are included in the Supporting Material. The determined choices for the phase factors of the DPPC-rich phase at 97% RH were [−1, −1, 1, −1, −1, −1, −1, −1, −1] for the 0% cholesterol sample, and [−1, −1, 1, −1, 1, −1, −1, −1, −1] for the 16, 20, and 25% cholesterol samples. Note that the only difference between these two sets of phases is the sign reversal for the fifth-order peak. This sign reversal is further supported by the fact that the fifth-order peak was missing in the 10% cholesterol sample. For the DOPC-rich phase, 4~6 orders of peaks were observed, and the phase factor choices were [−1, −1, 1, −1, 1, −1] for all. The diffraction patterns for samples with different cholesterol concentrations at 97% RH are shown in Fig. 1 *b*. Correct phase choices are crucial for the detailed data analysis needed to accurately estimate cholesterol content, described below in A New Method of Quantifying Cholesterol Content by Fitting EDPs.

Scaling

To normalize the relative electron density profiles to an absolute scale, the instrumental factor needs to be determined. The absolute density profile $\rho_{\text{absolute}}(z)$ is given by King et al. (31), King and White (35), and Jacobs and White (36),

$$\rho_{\text{absolute}}(z) = \rho_0 + \frac{1}{K}\rho_{\text{relative}}(z), \qquad (2)$$

where both the average density of the lipid ρ_0 and the instrumental factor K need to be determined. We obtain these two factors by comparing the EDP of our DPPC-rich phase from

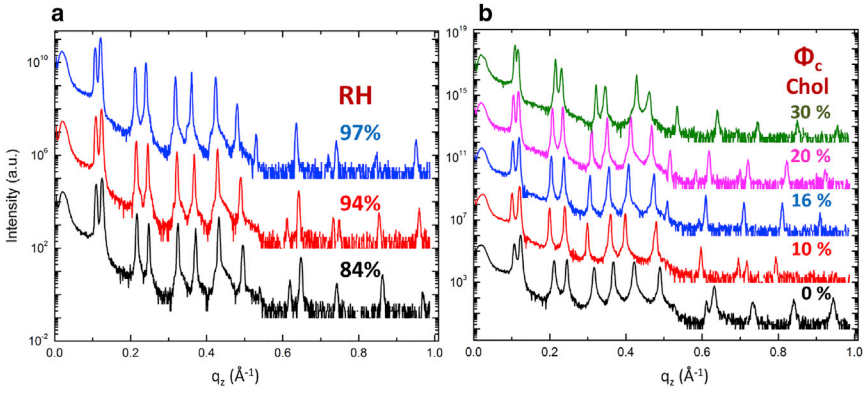

FIGURE 1 The diffraction patterns for (*a*) 0% cholesterol sample at different RH; (*b*) samples with different cholesterol content at 97% RH. To see this figure in color, go online.

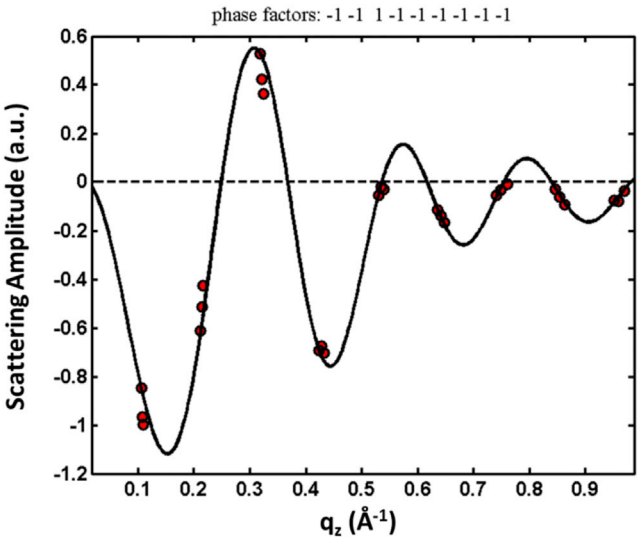

FIGURE 2 An example of a phasing diagram for the data in Fig. 1 *a*. Diffraction by a sample was measured at three different RHs to obtain the scattering amplitudes at a series of different lamellar spacings. The scattering amplitudes are either positive or negative. The phases are chosen such that the continuous form factor (*solid curve*) constructed from one set of data at one lamellar spacing goes through all other sets of data. To see this figure in color, go online.

the 0% cholesterol sample to the EDP of the pure DPPC obtained by Wiener et al. (34). As shown in Fig. 3 *a*, the EDPs are almost identical in the headgroup region and around the CH_3 groups. Furthermore, our EDP can resolve the plateau region of the DPPC tails, which we attribute to the higher orders of the diffraction peaks. The disagreement in the water region is most likely due to the differences in hydration: our data are measured under partial hydration while Weiner et al. (34) measured vesicles in excess water. While the multilayer samples that we investigated have <8 Å of water, vesicles in the study by Weiner et al. (34) have 25 Å, which then explains the presence of better resolved water regions in their profile.

The rest of the data were all normalized with the same two factors because the average lipid densities were similar and experimental conditions were identical, and we assume that cholesterol does not significantly change the average electron density in the bilayer unit cell. Comparisons of the EDPs for the different phases from samples with 0, 16, and 25% cholesterol are shown in Fig. 3, *b* and *c*. Even a casual inspection of the data reveals that the increase of the electron density at the lipid-chain region due to the added cholesterol in the DPPC-rich phase, is more than in the DOPC-rich phase, which we quantify in the next section.

A new method of quantifying cholesterol content by fitting EDPs

There are several methods in the literature regarding decomposition of the EDP into contributions from individ-

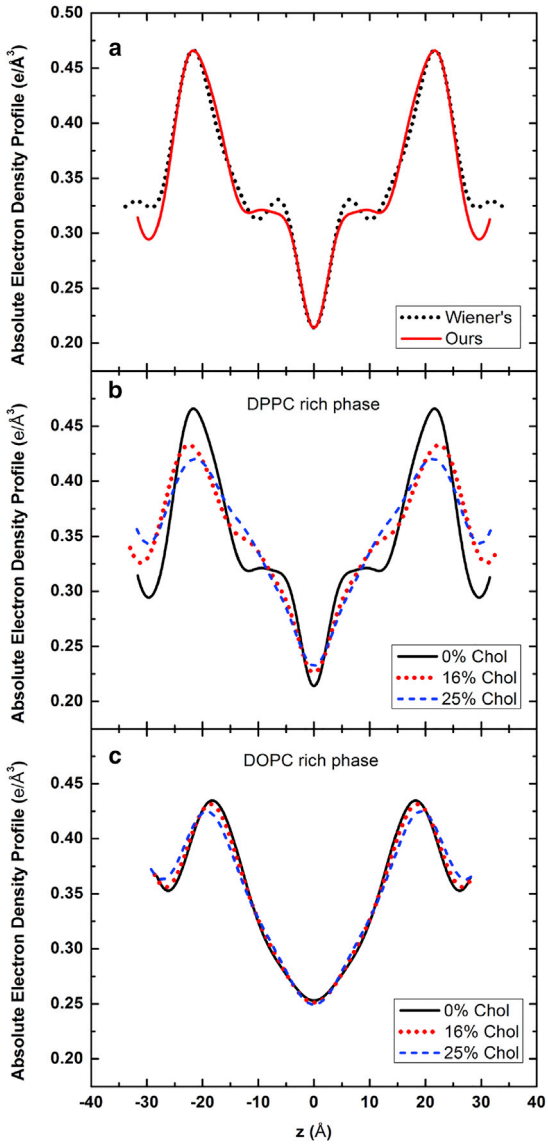

FIGURE 3 (*a*) Normalizing our EDP for the DPPC-rich phase of the sample with 0% cholesterol to Wiener and Nagle's absolute EDP for DPPC (34). (*b* and *c*) Comparison of the normalized EDPs for the samples with 0, 16, and 25% cholesterol ($\mathbf{\Phi_c}$) from the DPPC-rich phase and the DOPC-rich phase, respectively, on an absolute scale. To see this figure in color, go online.

ual components. Two popular ones are the 1G and 2G models, fit to either one or two Gaussian functions to the headgroup region, respectively, in addition to one Gaussian fitting of the methyl groups. Others, such as 4S and 5S strip models, interpret the profiles in terms of boxes (34). In our case, one could, in principle, fit every EDP with a 2G model plus an additional Gaussian for cholesterol, for example, to obtain a set of parameters for the headgroup, tailgroup, and cholesterol density. The parameters, so derived, can then be compared across the entire sample set consisting of lipid mixtures with systematically varied cholesterol content. Applying this approach,

however, would lead to overparameterization: each EDP fitted with four Gaussians (two for headgroup of the asymmetric shape, one for the methyl group, and one for cholesterol) plus a constant baseline, will generate 12 independent parameters (the position for methyl group is taken as 0). Fitting the EDP to such a heavily parameterized model will obviously result in broad ranges of fitting parameters, losing unique solutions, thereby rendering the analysis less meaningful. To circumvent this issue and find a minimal set of parameters, which adequately quantifies the change in the cholesterol content, we have developed a new (to our knowledge) fitting method. We call it the basic lipid profile (BLP) scaling method. The essence of this method is to eliminate redundant parameters by keeping the basic lipid structure proportions fixed.

BLP generation based on modified 2G model

After cooling down to room temperature, the sample with 0% cholesterol phase separates into a DPPC-rich gel phase and a DOPC-rich fluid phase. Our method is based on generating a BLP by fitting the EDPs of the respective phases of the sample with 0% cholesterol. One can use conventional methods for this fitting, using either the 1G or 2G model, depending on the headgroup shape. In our case, we used the 2G model with one baseline. The electron density profile is decomposed into two Gaussians for the headgroup (G_1, G_2), with one Gaussian for the methyl group (G_3) and one constant baseline C_B:

$$\rho_0(z) = C_B + \sum_{n=1}^{3} G_n, \tag{3}$$

where $G_n = a_n \exp(-((z-b_n)^2/2c_n^2)), n = 1,2,3$. Note that a_3 is negative. The fitting parameters are listed in Table 1. The fits for the DPPC-rich and DOPC-rich phases are shown in Fig. 4, *a* and *b* (*top*), respectively.

Scaling of BLP: minimizing the fitting parameters

With the fitted parameters for the BLPs for each of the phases, we can start fitting the EDPs for samples with added cholesterol. We use two scaling parameters for the BLP: the overall amplitude scaling factor C_1, and Gaussian width scaling factor C_2. The scaling factor for the Gaussian position was fixed to (D_{hh}/D^o_{hh}), where D_{hh} is the phosphate-to-phosphate distance (PtP) for the sample with added cholesterol (determined as the distance between two maximums on the EDP), and D^o_{hh} is the PtP for the 0% cholesterol sample (BLP sample). The functional form for the scaled BLP is as follows (compare with Eq. 3):

$$\rho_{BLP}(z) = C_1\left[\frac{d_o}{d}C_B + \frac{1}{C_2}\sum_{n=1}^{3} a_n \exp\left(-\frac{\left(z - \frac{D_{hh}}{D^o_{hh}}b_n\right)^2}{2(C_2 c_n)^2}\right)\right]. \tag{4}$$

The (d_o/d) factor in the first term and the $(1/C_2)$ factor in the second term ensure that the integrated area under the density profile represented by the expression inside the square bracket is constant. Physically, C_1 models the overall electron density change due to looser or denser packing; C_2 models the smearing of electron density profile due to roughness, disorder, or fluctuations.

After the scaled BLP is constructed, we can write out the equation for fitting the EDPs with added cholesterol as

$$\rho(z) = \rho_{BLP}(z) + \Delta\rho_{Chol}, \tag{5}$$

where $\Delta\rho_{Chol} = a_{Chol}\exp(-((z-b_{Chol})^2/2c^2_{Chol}))$ is the Gaussian representing the increased electron density due to the added cholesterol.

The EDPs of samples with added cholesterol are thus fitted with the two scaling factors C_1 and C_2, and three parameters for $\Delta\rho_{Chol}$, for a total of five free parameters. It turned out to be unnecessary to change the value of the parameter C_B with cholesterol concentration to achieve a good fit to the EDPs, so they were held constant although different for each of the phases.

This result of the fitting allows us to quantitatively compare the EDPs of the samples with added cholesterol to the ones without cholesterol. The fittings in the middle

TABLE 1 Gaussian Fitting Results of Gel Phase and Fluid Phase EDP with 0% Cholesterol

	Constant Baseline	Tail Region	Head Region I	Head Region II
Gel Phase (DPPC-Rich)				
Baseline (e/Å^3)	0.319 ± 0.002	—	—	—
Height (e/Å^3)	—	−0.106 ± 0.002	0.085 ± 0.005	0.130 ± 0.005
Width (Å)	—	2.3 ± 0.1	2.3 ± 0.1	2.3 ± 0.1
Position (Å)	—	—	18.1 ± 0.3	22.5 ± 0.3
Fluid Phase (DOPC-Rich)				
Baseline (e/Å^3)	0.289 ± 0.002	—	—	
Height (e/Å^3)	—	−0.036 ± 0.002	0.062 ± 0.005	0.114 ± 0.005
Width (Å)	—	3.8 ± 0.1	3.8 ± 0.1	4.0 ± 0.1
Position (Å)	—	—	14.6 ± 0.3	19.7 ± 0.3

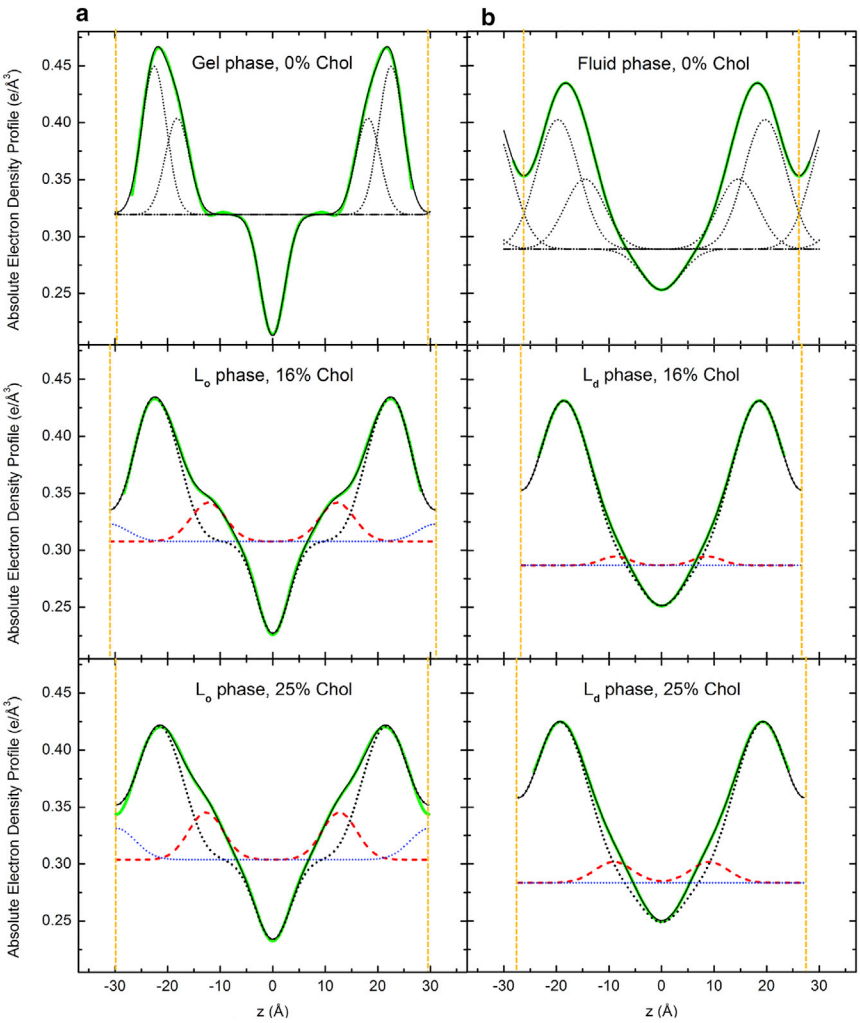

FIGURE 4 The fitting of 0, 16, and 25% cholesterol sample EDPs of the DPPC-rich phase (*a*) and the DOPC-rich phase (*b*) using the BLP scaling method. The pair of yellow vertical dotted lines indicate one period of the unit cell, namely the *d*-spacing. The solid green line is the EDP generated from diffraction measurements. The solid black line is the fitted curve. The top figures are the BLP fitting of the 0% cholesterol sample using the 2G model. The dotted black lines are the Gaussian components and the constant baseline. The middle and bottom figures are the fittings of cholesterol content for the 16 and 25% cholesterol samples with the scaled BLP obtained from the 0% cholesterol EDP fitting. The dotted black lines are the BLP values scaled from (*a*). The red dashed lines are the Gaussian fits of the electron density increase due to added cholesterol. The blue dotted lines are the additional water smear into the outer headgroups due to the change of lipid packing. To see this figure in color, go online.

and lower figures of Fig. 4 show the EDPs of each phase derive from the samples with 16 and 25% cholesterol, respectively. The green solid lines are the Fourier-constructed EDPs from diffraction measurements, the dotted black lines are the scaled BLPs, the red dashed lines are Gaussian fits of the electron density increase due to added cholesterol, and the black solid lines are the total fitted curves. The blue dotted line marks the additional density of water at the outer side of the headgroup added due to the change in lipid packing, and our results are not sensitive to this parameter because the cholesterol sits at the tailgroup side. The fitted results for all cholesterol concentrations are listed in Table 2.

Distribution of cholesterol between saturated and unsaturated lipids

The increased electron densities resulting from the fitting are due to the ring structures in the cholesterol molecule. This increase in terms of the electron density per unit area $\Delta\delta$ is calculated as the integrated area of $\Delta\rho_{\mathrm{Chol}}$,

$$\Delta\delta = \int_{-d/2}^{d/2} \Delta\rho_{\mathrm{Chol}} dz. \tag{6}$$

The plot of $\Delta\delta$ versus initial cholesterol concentration $\mathbf{\Phi_c}$ is plotted in Fig. 5 *a*. Note that this is not the integrated electron density of cholesterol molecules, but rather the averaged electron density difference at the chain region after adding cholesterol. To determine how the cholesterol partitions between the two (DOPC and DPPC) lipids, we carried out the following calculation. Assuming that the electron density differences between the cholesterol ring structure and the lipid chain region are roughly the same for the L_o and L_d phases, the amount of the cholesterol in each phase would be proportional to the averaged difference $\Delta\delta$ multiplied by the phase volume percentage φ. Thus, the percentage of cholesterol partitioned into L_o phase is

$$\vartheta_{\mathrm{L_o}} = \frac{\Delta\delta_{\mathrm{L_o}} \times \varphi_{\mathrm{L_o}}}{\Delta\delta_{\mathrm{L_o}} \times \varphi_{\mathrm{L_o}} + \Delta\delta_{\mathrm{L_d}} \times \varphi_{\mathrm{L_d}}}, \tag{7}$$

TABLE 2 Fitting Results of the Scaling Factors C_1, C_2, and the Gaussian Height, Width, and Position for the Increased Electron Density due to Cholesterol

Φ_c (Initial Chol %)	C_1 ($\pm$0.005)	C_2 ($\pm$0.01)	Chol Gaussian Height (e/Å^3) ($\pm$0.001 e/Å^3)	Chol Gaussian Width (Å) ($\pm$0.1Å)	Chol Gaussian Position (Å) ($\pm$0.5Å)
L_o Phase (DPPC-Rich)					
10	1.038	1.36	0.032	3.0	10.2
16	1.008	1.33	0.034	3.3	12.2
20	0.993	1.33	0.039	3.2	11.6
25	0.956	1.45	0.041	3.3	12.7
30	0.947	1.48	0.046	3.3	12.7
L_d Phase (DOPC-Rich)					
10	1.000	1.00	0	—	—
16	1.010	1.02	0.008	2.8	8.8
20	1.013	1.03	0.014	3.0	9.1
25	1.021	1.06	0.018	3.5	9.1
30	1.008	1.07	0.023	3.8	9.2

while for the L_d phase, the fractional cholesterol content is the reminder of the total:

$$\vartheta_{L_d} = 1 - \vartheta_{L_o}. \tag{8}$$

The plot for the cholesterol partition is shown in Fig. 5 *b*, with φ in the inset. The φ was taken as proportional to the ratio of the sum of the integrated intensities of diffraction peaks in each phase. Here we measured integrated intensity ratios for $\mathbf{\Phi_c}$ of 16 and 25%, and linearly interpolated for the remaining concentrations.

The concentration of cholesterol in L_o and L_d phase after phase separation would be

$$x_{L_o/L_d} = \frac{\vartheta_{L_o/L_d} \times \mathbf{\Phi_c}}{\varphi_{L_o/L_d}} \tag{9}$$

and the plot is shown in Fig. 5 *c* with linear fits. The fitting results are in Table 3.

Note that this result indicates that the cholesterol only starts to partition into the L_d phase when $\mathbf{\Phi_c}$ is >10%, below which almost all the cholesterol segregates into the L_o phase.

The distribution coefficient K, defined as the ratio of concentration of the two phases, is plotted in Fig. 5 *d*:

$$K = \frac{x_{L_o}}{x_{L_d}}. \tag{10}$$

If x is linear with respect to $\mathbf{\Phi_c}$, then

$$K = \frac{a_1 + b_1\mathbf{\Phi_c}}{a_2 + b_2\mathbf{\Phi_c}}. \tag{11}$$

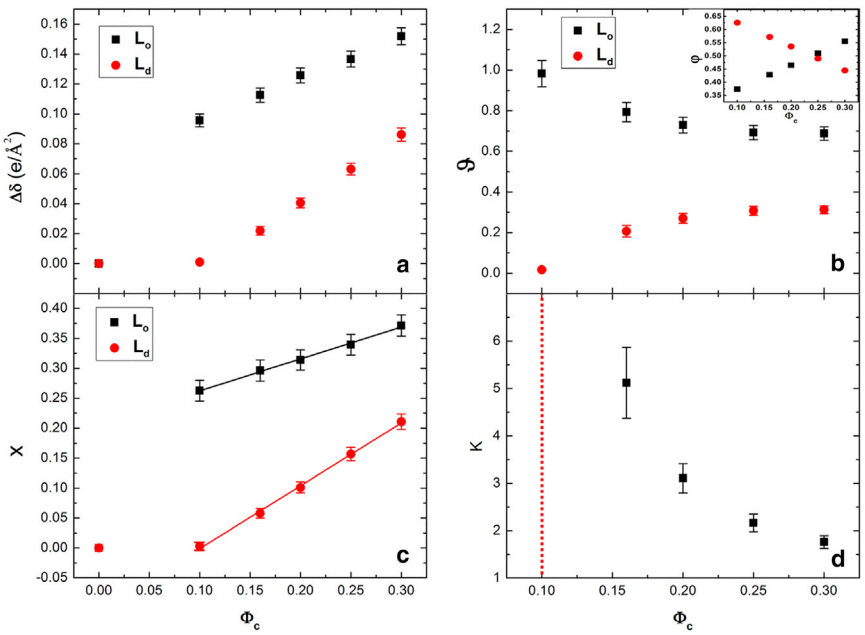

FIGURE 5 (*a*) Plots of additional electron density/unit area due to cholesterol $\Delta\delta$ versus $\mathbf{\Phi_c}$; (*b*) cholesterol partition ϑ versus $\mathbf{\Phi_c}$ with phase volume fraction φ (*inset*); (*c*) cholesterol concentration x fitted with linear functions for each phase; (*d*) distribution coefficient K versus $\mathbf{\Phi_c}$. The dashed vertical line at $\mathbf{\Phi_c} = 0.10$ indicates that because within experimental error, x for the L_d phase was zero, K is some large (undetermined) number. To see this figure in color, go online.

TABLE 3 Linear Fitting Results of *x*

	a (Intersect)	*b* (Slope)
x_{L_o}	0.22 ± 0.02	0.5 ± 0.1
x_{L_d}	−0.11 ± 0.01	1.1 ± 0.1

Previously, Veatch et al. (37) have mapped out a phase diagram for the DOPC and DPPC with cholesterol using NMR and measured the two tie lines across 1:1 DOPC/DPPC with 15 and 20% cholesterol at 25°C, of which the partitioning of cholesterol into the L_o and L_d phases is, respectively, 26 and 9% for the 15% cholesterol and 31 and 11% for the 20% cholesterol. Comparing our result of 16 and 20% to these values, of which the partitioning of cholesterol into the L_o and L_d phases is 29 and 6% for the 16% cholesterol and 31 and 10% for the 20% cholesterol, we find an excellent agreement, within experimental error, between the cholesterol concentration in each phase estimated from our fitting and their NMR results.

We also tried to compare our results with the study of Heftberger et al. (11), which mapped out two tie lines of the phase diagram of DOPC/DPPC/CHOL mixture at 15°C, as well as 15~30°C in their supporting materials. We find that for a starting mixture of 1:1 DOPC/DPPC with 20% cholesterol, the partitioning of cholesterol into the Lo and Ld phases is, respectively, 31 and 10% at 25°C; and upon extrapolating measured points from Heftberger et al. (11) in the ternary phase diagram, we find the corresponding values are 28 and 13%, respectively, at 25°C, which is also very close.

There is one discrepancy at 10% cholesterol between our result and that of Veatch et al. (37), in that we observed the L_o phase and they observed the gel phase for the DPPC-rich phase. This is because 10% cholesterol is likely to be very close to the phase boundary between the gel phase (<10% cholesterol) and liquid-ordered phase (>10% cholesterol) in the phase diagram for the DPPC-rich component at 25°C. In our samples, from the PtP measurement shown in Fig. 6, it is clear that this phase is closer to the liquid-ordered phase than the gel phase. The discrepancy may be due to a slight difference in the actual cholesterol concentrations.

Condensing effect

Fig. 6 *a* shows the measured PtP versus $\mathbf{\Phi_c}$ plot. We can see that at >10% $\mathbf{\Phi_c}$, where the DPPC-rich phase is in the L_o phase instead of the gel phase, the added cholesterol increases the bilayer thickness of the L_d phase while it decreases the bilayer thickness of the L_o phase. This is known as the **"**cholesterol-condensing effect**".** In this ternary mixture, it is consistent with the theory and results on binary systems given by Hung et al. (16), who showed that the hydrophobic regions of lipids tend to match the hydrophobic thickness of the cholesterol. In our case, the hydrophobic thickness of cholesterol is intermediate between the chain lengths of the DPPC and the DOPC, and therefore the bilayers in the L_o phase are thinned and the bilayers in the L_d phase are thickened after adding cholesterol.

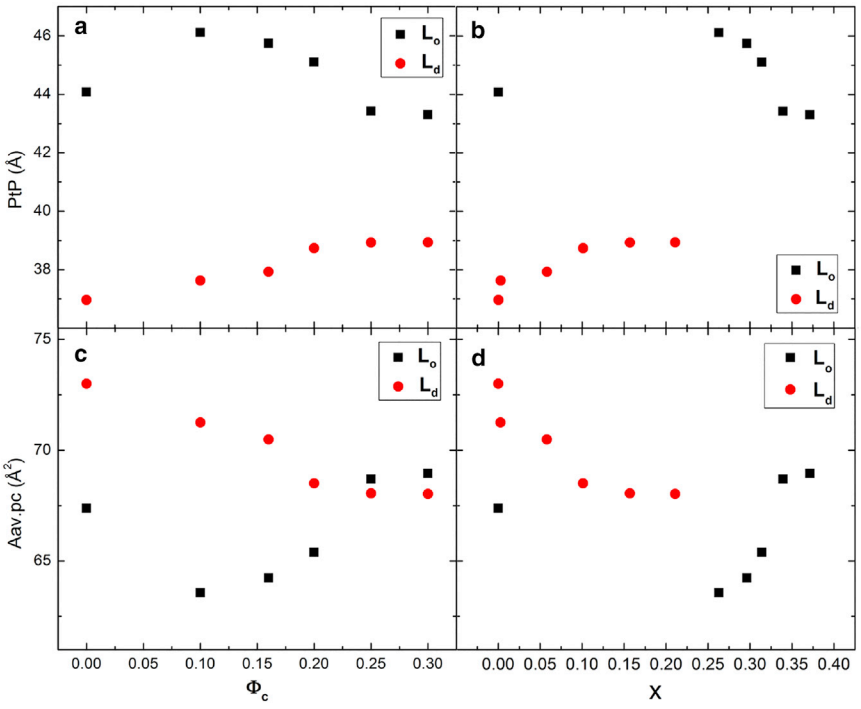

FIGURE 6 (*a*) Phosphate to phosphate distance PtP versus $\mathbf{\Phi_c}$, the total cholesterol content in the sample. (*b*) PtP versus *x*, the cholesterol concentration in the respective phase. (*c*) The average cross-section area of phospholipid versus $\mathbf{\Phi_c}$. (*d*) The average cross-section area of phospholipid versus *x*. The error bars are smaller than the symbol sizes. To see this figure in color, go online.

We can also calculate the average molecular area in each phase according to Hung et al. (16):

$$A_{\mathrm{av}} = xA_{\mathrm{cho}} + (1-x)A_{\mathrm{av.pc}}, \tag{12}$$

where x is the cholesterol concentration in that phase, $A_{\mathrm{cho}} \approx 39$ Å^2 was taken from monolayer measurements on pure cholesterol (38,39), and $A_{\mathrm{av.pc}}$ is the average cross-section area of phospholipid in that phase, calculated by

$$A_{\mathrm{av.pc}} = \frac{2V_c}{PtP - 10}. \tag{13}$$

Here V_c is the chain volume of the lipid; 10 Å is twice the length of the glycerol region. The value $A_{\mathrm{av.pc}}$ is plotted in Fig. 6 *c*. For V_c, we choose to use the chain volume of the majority lipid in the particular phase under consideration: DOPC chain volume (984 Å^3) for the DOPC-rich phase (40) and literature DPPC chain volume (1148 Å^3) for the DPPC-rich phase (41).

Also the PtP and $A_{\mathrm{av.pc}}$ can be plotted versus x, the concentration of cholesterol in each phase after phase separation (Fig. 6, *b* and *d*), which can be better compared to the binary system results. We can see that the change of PtP in the L_o phase is more than that of the L_d phase, which agrees well with the results by Hung et al. (16) of binary systems with saturated (DMPC) and unsaturated (DOPC) lipids. Note that here the DPPC has longer chain length than the DMPC, which leads to a thinning effect caused by the cholesterol rather than a thickening effect for the DMPC. The thinning effect of cholesterol in the DPPC-rich L_o phase is consistent with the observation made by Mills et al. (28) on multilamellar vesicles (Fig. 6, *bottom row*, 25°C). The average molecular area of the L_o phase slightly goes up because of the conservation of the volume of the lipid molecule, which deviates from the simulation by Edholm and Nagle (18) for the DPPC/cholesterol binary systems. Similarly, the average molecular area of the L_d phase goes down because of the stretching of the DOPC molecule with increased cholesterol concentration.

We note that the PtP measurement is a good measure of the cholesterol condensing effect on lipids. The result of average molecular area versus local cholesterol concentration is in good agreement with the literature: the average molecular area of the L_d phase agrees well with DOPC results by Hung et al. (16); the average molecular area of the L_o phase is very close to the neutron result for 32.5% cholesterol of Armstrong et al. (19).

Cholesterol position

The fitting localizes the cholesterol packing distribution with great precision. Fig. 7 shows the maximum position of fitted cholesterol distribution for both the L_o and the L_d phases: the cholesterol ring structure is mostly concentrated at 12.3 Å for the L_o phase and 9 Å for the L_d phase from the bilayer center. Although the difference of PtP between the two phases is ~2~4 Å, if one aligns the electron density profiles of the two with the headgroups, one can see that the cholesterol sits roughly at the same position, as shown in the cartoon on the right side in Fig. 7. This result agrees with the previous study of McIntosh (17) on cholesterol packing of saturated lipids with different chain lengths. Several other studies (21,22,42) have also indicated that the hydroxyl group of cholesterol must be in very close proximity to the carbonyl group of the lipids.

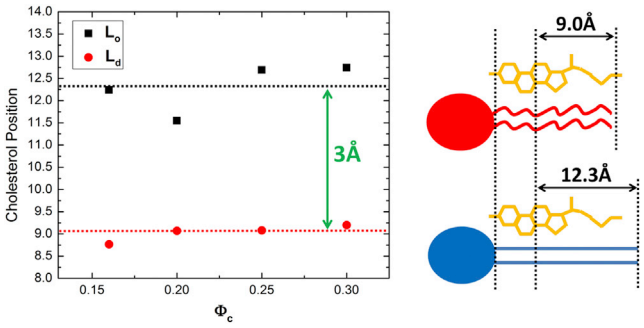

FIGURE 7 Cholesterol position plot (*left*) agrees with the cholesterol packing along the hydrophobic surface of lipids (as shown in the cartoon on the *right*). The statistical error of cholesterol position in the plot is estimated to be ±0.7 Å. To see this figure in color, go online.

Change of lipid packing

The change of packing is reflected in the two scaling factors: C_1 scales with the electron density and hence reflects the change in the area occupied per lipid, and thus the overall change in the lipid packing density; C_2 reflects the smearing of the EDP, which might be due to increased fluctuation or roughness. The factor C_2 will be referred to as the "disorder parameter".

From the plot showing the variation of C_1 with initial cholesterol content in Fig. 8 *a*, we can see that the overall packing density decreases for the L_o phase, while it increases for the L_d phase as a function of $\mathbf{\Phi_c}$. This is mostly due to the change of PtP: in the DPPC-rich L_o phase, as cholesterol is added, the bilayer thickness decreases and because the lipid volume stays approximately constant, the area per lipid increases. On the other hand, in the DOPC-rich L_d phase, which has an increased bilayer thickness, the lipids are stretched so the packing density increases.

The plot showing the variation of C_2 with initial cholesterol content $\mathbf{\Phi_c}$ in Fig. 8 *b* gives additional information. The smearing of the EDP while maintaining its integrated area means increased fluctuation or roughness (disorder). It has been known since Levine and Wilkins (43) that the EDPs of cholesterol-containing membranes do not smear with increasing hydration, implying lessened fluctuations of the bilayers, which means that the cholesterol will stiffen the bilayers. Therefore, this smearing of EDP that we observe

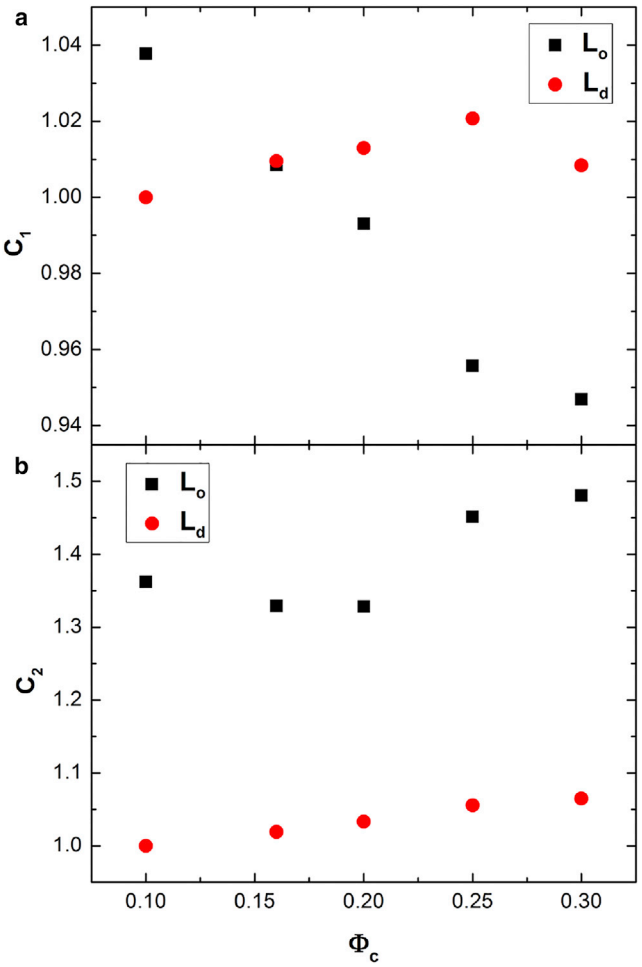

FIGURE 8 (*a*) The scaling factor for the overall electron density amplitude C_1 plotted versus $\mathbf{\Phi_c}$. (*b*) The scaling factor of Gaussian width C_2 versus $\mathbf{\Phi_c}$. The error bars are comparable to the symbol sizes. To see this figure in color, go online.

must come from the increased roughness resulted from the disordering effect of adding cholesterol. While $C_2 = 1$ for the cholesterol-free samples, after adding cholesterol the averaged lipid bilayer roughness for the DOPC-rich L_d phase changes very little. However, the DPPC-rich L_o phase increases by >30% for $\mathbf{\Phi_c} = 10$~20%, and increases by another 15% for $\mathbf{\Phi_c} = 25$ and 23% for $\mathbf{\Phi_c} = 30\%$. The initial increase at $\mathbf{\Phi_c} = 10\%$ from $C_2 = 1$ to $C_2 = 1.36$ is due to the gel-fluid phase transition. The second increase at $\mathbf{\Phi_c} = 20\%$ appears to indicate some further major change in the packing of the lipid molecules. At $\mathbf{\Phi_c} = 20\%$, the cholesterol concentration in the L_o phase is ~30%, as shown in Fig. 5 *c*. This may be correlated with the sudden increase in the interchain spacing after $x = 30\%$, as indicated by wide-angle x-ray scattering measurement by Mills et al. (44). As noted by Hung et al. (16), after cholesterol complexing saturates after 38% cholesterol, more cholesterol would still go into the sample as free cholesterol. This sudden change in chain packing after 30% cholesterol can be caused by the increased amount of free cholesterol when the amount of complexing cholesterol is close to saturation. The saturation of the complexing cholesterol is also indicated by the PtP measurement in Fig. 6.

DISCUSSION

In summary, the, to our knowledge, newly developed BLP scaling method is shown to be useful in the quantitative analysis of the relatively subtle changes in the EDPs of the L_o and L_d phases with increasing cholesterol content. With this analysis method, we can localize the added component (in this case cholesterol) with high accuracy and quantify the resulting increase of electron density, as well as the changes in lipid packing. We can then quantify the partition of cholesterol into the two phases, as we hope we have demonstrated in this article.

We have determined the cholesterol concentrations x in each of the L_o and L_d phases as a function of the initial cholesterol concentration $\mathbf{\Phi_c}$. For the 10% cholesterol ($\mathbf{\Phi_c} = 10\%$) in the sample, we could not detect cholesterol in the L_d phase within our experimental error. Similar observations have been made by others (45). The cholesterol distribution coefficient is found to obey a simple relation to $\mathbf{\Phi_c}$ as shown in Eq. 11. In our studies of the 10 and 16% cholesterol samples, we did not observe any three-phase coexistence over repeated experiments. This result disagrees with results by Chen et al. (13) obtained for multilamellar vesicles using a synchrotron source. We postulate that it might be due to the nonhomogeneous or nonequilibrium conditions of their vesicle samples.

One thing worth mentioning is that all samples were measured at 25°C except for the 30% cholesterol sample, which was measured at 11°C due to a lower phase transition temperature. However, we still get very smooth curves as shown in Fig. 5. According to extrapolated values from phase diagrams in Heftberger et al. (11), the partitions of cholesterol of 1:1 DOPC/DPPC with 20% cholesterol at 15°C are 28 and 12% in the L_o and L_d phases, respectively, while at 20°C they are 28 and 13%, respectively, which are almost the same. From these results and our own, it is quite likely that within the measurement accuracy, the partition of cholesterol is not very sensitive to temperature.

The measured PtP show that the condensing effect for the DPPC-rich L_o phase is stronger than for the DOPC-rich L_d phase, which supports previous studies of the condensing effect by Hung et al. (16). The average molecular area is calculated according to the measured PtP values from Eqs. 12 and 13.

The position of the maximum in the electron density in the cholesterol ring was measured for both the L_o and L_d phases to be ~12 and 9 Å from the bilayer center. These numbers support the previous studies of the cholesterol packing behavior, which show that the cholesterol molecules align themselves

with the interface between the hydrophilic headgroups and hydrophobic tailgroups of the lipids.

The disorder of the lipid packing as a function of initial cholesterol concentration is quantified for both phases. The disorder increases by 36% upon adding 10% cholesterol to the sample for the DPPC-rich L_o phase, while no change is found for the DOPC-rich L_d phase. This significant increase of disorder in the DPPC-rich phase is mainly due to a change from the gel phase to the liquid-ordered phase. For $\mathbf{\Phi_c} >$ 10%, the disorder of the L_o phase stays roughly the same (decreasing by 3%) until $\mathbf{\Phi_c} = 20\%$, after which the disorder increases again by another 12~15% for $\mathbf{\Phi_c} = 25\%$ and $\mathbf{\Phi_c} = 30\%$. This indicates that another major change in packing occurs in the L_o phase around $\mathbf{\Phi_c} = 20\%$, which may be due to a dramatic increase in the interchain spacings. For the L_d phase, the total increase of the disorder parameter is ~6%.

SUPPORTING MATERIAL

Four figures are available at http://www.biophysj.org/biophysj/supplemental/S0006-3495(16)00210-1.

AUTHOR CONTRIBUTIONS

Y.M. designed the experiments, performed experiments, built the model, analyzed data, and wrote the initial draft of the article; S.K.G. contributed to the initial phasing analytic tool; D.A.D. prepared the samples for the experiment; S.B. contributed to the error analysis and suggested improvements in figure plotting; S.K.S., L.B.L., and A.N.P. provided intellectual and technical guidance; S.K.S. is the principle investigator of the supporting grant; and Y.M., S.K.G., S.B., L.B.L., A.N.P., and S.K.S. contributed to revising and improving the article.

ACKNOWLEDGMENTS

This work was supported by the Office of Basic Energy Sciences, U.S. Department of Energy under Department of Energy grant No. DE-FG02-04ER46173.

REFERENCES

1. Brown, D. A., and J. K. Rose. 1992. Sorting of GPI-anchored proteins to glycolipid-enriched membrane subdomains during transport to the apical cell surface. *Cell.* 68:533–544.
2. Simons, K., and E. Ikonen. 1997. Functional rafts in cell membranes. *Nature.* 387:569–572.
3. Simons, K., and E. Ikonen. 2000. How cells handle cholesterol. *Science.* 290:1721–1726.
4. Lingwood, D., H.-J. Kaiser, …, K. Simons. 2009. Lipid rafts as functional heterogeneity in cell membranes. *Biochem. Soc. Trans.* 37:955–960.
5. Leathes, J. 1925. Condensing effect of cholesterol on monolayers. *Lancet.* 208:853–856.
6. Veatch, S. L., and S. L. Keller. 2002. Organization in lipid membranes containing cholesterol. *Phys. Rev. Lett.* 89:268101.
7. Veatch, S. L., and S. L. Keller. 2003. Separation of liquid phases in giant vesicles of ternary mixtures of phospholipids and cholesterol. *Biophys. J.* 85:3074–3083.
8. Veatch, S. L., and S. L. Keller. 2005. Miscibility phase diagrams of giant vesicles containing sphingomyelin. *Phys. Rev. Lett.* 94:148101.
9. Veatch, S. L., K. Gawrisch, and S. L. Keller. 2006. Closed-loop miscibility gap and quantitative tie-lines in ternary membranes containing diphytanoyl PC. *Biophys. J.* 90:4428–4436.
10. Veatch, S. L., I. V. Polozov, …, S. L. Keller. 2004. Liquid domains in vesicles investigated by NMR and fluorescence microscopy. *Biophys. J.* 86:2910–2922.
11. Heftberger, P., B. Kollmitzer, …, G. Pabst. 2015. In situ determination of structure and fluctuations of coexisting fluid membrane domains. *Biophys. J.* 108:854–862.
12. Uppamoochikkal, P., S. Tristram-Nagle, and J. F. Nagle. 2010. Orientation of tie-lines in the phase diagram of DOPC/DPPC/cholesterol model biomembranes. *Langmuir.* 26:17363–17368.
13. Chen, L., Z. Yu, and P. J. Quinn. 2007. The partition of cholesterol between ordered and fluid bilayers of phosphatidylcholine: a synchrotron x-ray diffraction study. *Biochim. Biophys. Acta.* 1768:2873–2881.
14. Barrett, M. A., S. Zheng, …, M. C. Rheinstädter. 2013. Solubility of cholesterol in lipid membranes and the formation of immiscible cholesterol plaques at high cholesterol concentrations. *Soft Matter.* 9:9342–9351.
15. Alsop, R. J., C. L. Armstrong, …, M. C. Rheinstädter. 2015. Cholesterol expels ibuprofen from the hydrophobic membrane core and stabilizes lamellar phases in lipid membranes containing ibuprofen. *Soft Matter.* 11:4756–4767.
16. Hung, W.-C., M.-T. Lee, …, H. W. Huang. 2007. The condensing effect of cholesterol in lipid bilayers. *Biophys. J.* 92:3960–3967.
17. McIntosh, T. J. 1978. The effect of cholesterol on the structure of phosphatidylcholine bilayers. *Biochim. Biophys. Acta.* 513:43–58.
18. Edholm, O., and J. F. Nagle. 2005. Areas of molecules in membranes consisting of mixtures. *Biophys. J.* 89:1827–1832.
19. Armstrong, C. L., D. Marquardt, …, M. C. Rheinstädter. 2013. The observation of highly ordered domains in membranes with cholesterol. *PLoS One.* 8:e66162.
20. Pabst, G., N. Kučerka, …, J. Katsaras. 2010. Applications of neutron and x-ray scattering to the study of biologically relevant model membranes. *Chem. Phys. Lipids.* 163:460–479.
21. Worcester, D. L., and N. P. Franks. 1976. Structural analysis of hydrated egg lecithin and cholesterol bilayers. II. Neutron diffraction. *J. Mol. Biol.* 100:359–378.
22. Franks, N. P. 1976. Structural analysis of hydrated egg lecithin and cholesterol bilayers. I. X-ray diffraction. *J. Mol. Biol.* 100:345–358.
23. Kučerka, N., S. Tristram-Nagle, and J. F. Nagle. 2006. Closer look at structure of fully hydrated fluid phase DPPC bilayers. *Biophys. J.* 90:L83–L85.
24. Klauda, J. B., N. Kučerka, …, J. F. Nagle. 2006. Simulation-based methods for interpreting x-ray data from lipid bilayers. *Biophys. J.* 90:2796–2807.
25. Kučerka, N., J. D. Perlmutter, …, J. N. Sachs. 2008. The effect of cholesterol on short- and long-chain monounsaturated lipid bilayers as determined by molecular dynamics simulations and x-ray scattering. *Biophys. J.* 95:2792–2805.
26. Li, C., D. Constantin, and T. Salditt. 2004. Biomimetic membranes of lipid–peptide model systems prepared on solid support. *J. Phys. Condens. Matter.* 16:S2439–S2453.
27. Tayebi, L., Y. Ma, …, A. N. Parikh. 2012. Long-range interlayer alignment of intralayer domains in stacked lipid bilayers. *Nat. Mater.* 11:1074–1080.
28. Mills, T. T., S. Tristram-Nagle, …, G. W. Feigenson. 2008. Liquid-liquid domains in bilayers detected by wide angle x-ray scattering. *Biophys. J.* 95:682–690.
29. Ma, Y., S. K. Ghosh, …, S. K. Sinha. 2015. Accurate calibration and control of relative humidity close to 100% by x-raying a DOPC multilayer. *Phys. Chem. Chem. Phys.* 17:3570–3576.
30. Caille, A. 1972. Remarques sur la diffusion des rayons x dans les smectiques. *CR Acad. Sci. Paris Sér. B.* 274:891–893.

31. King, G. I., R. E. Jacobs, and S. H. White. 1985. Hexane dissolved in dioleoyllecithin bilayers has a partial molar volume of approximately zero. *Biochemistry.* 24:4637–4645.

32. Blaurock, A. E. 1971. Structure of the nerve myelin membrane: proof of the low-resolution profile. *J. Mol. Biol.* 56:35–52.

33. Ghosh, S. K., S. Aeffner, and T. Salditt. 2011. Effect of PIP_2 on bilayer structure and phase behavior of DOPC: an x-ray scattering study. *ChemPhysChem.* 12:2633–2640.

34. Wiener, M. C., R. M. Suter, and J. F. Nagle. 1989. Structure of the fully hydrated gel phase of dipalmitoylphosphatidylcholine. *Biophys. J.* 55:315–325.

35. King, G. I., and S. H. White. 1986. Determining bilayer hydrocarbon thickness from neutron diffraction measurements using strip-function models. *Biophys. J.* 49:1047–1054.

36. Jacobs, R. E., and S. H. White. 1989. The nature of the hydrophobic binding of small peptides at the bilayer interface: implications for the insertion of transbilayer helices. *Biochemistry.* 28:3421–3437.

37. Veatch, S. L., O. Soubias, …, K. Gawrisch. 2007. Critical fluctuations in domain-forming lipid mixtures. *Proc. Natl. Acad. Sci. USA.* 104:17650–17655.

38. Phillips, M. 1972. The physical state of phospholipids and cholesterol in monolayers, bilayers, and membranes. *Prog. Surf. Membr. Sci.* 5:139–221.

39. Scheffer, L., I. Solomonov, …, L. Addadi. 2005. Structure of cholesterol/ceramide monolayer mixtures: implications to the molecular organization of lipid rafts. *Biophys. J.* 88:3381–3391.

40. Nagle, J. F., and S. Tristram-Nagle. 2000. Structure of lipid bilayers. *Biochim. Biophys. Acta.* 1469:159–195.

41. Greenwood, A. I., S. Tristram-Nagle, and J. F. Nagle. 2006. Partial molecular volumes of lipids and cholesterol. *Chem. Phys. Lipids.* 143:1–10.

42. Franks, N. P., and W. R. Lieb. 1979. The structure of lipid bilayers and the effects of general anaesthetics. An x-ray and neutron diffraction study. *J. Mol. Biol.* 133:469–500.

43. Levine, Y. K., and M. H. F. Wilkins. 1971. Structure of oriented lipid bilayers. *Nat. New Biol.* 230:69–72.

44. Mills, T. T., J. Huang, …, J. F. Nagle. 2009. Effects of cholesterol and unsaturated DOPC lipid on chain packing of saturated gel-phase DPPC bilayers. *Gen. Physiol. Biophys.* 28:126–139.

45. de Joannis, J., P. S. Coppock, …, J. T. Kindt. 2011. Atomistic simulation of cholesterol effects on miscibility of saturated and unsaturated phospholipids: implications for liquid-ordered/liquid-disordered phase coexistence. *J. Am. Chem. Soc.* 133:3625–3634.